Research Article

Muhammad Zahid, Fateh Ali*, Basma Souayeh*, and Muhammad Tahir Khan

Influence of variable viscosity on existing sheet thickness in the calendering of non-isothermal viscoelastic materials

https://doi.org/10.1515/phys-2024-0023
received December 23, 2023; accepted April 19, 2024

Abstract: The calendering process is pivotal in enhancing various materials' surface properties and characteristics, making them indispensable for achieving desired product quality and performance. Also, this process holds significant relevance in various industrial applications, such as polymer processing, food production, and the manufacturing of composite materials. So, the aim of this study is to theoretically examine the calendering process applied to third-grade materials. It specifically explores how temperature variations impact material behavior during passage through two counter-rotating heated rolls. Particular consideration is given to the influence of temperature-dependent viscosity *via* Reynold's model. The complexities of mass, momentum, and energy balance equations are reduced through the application of the Lubrication approximation theory. Solutions to these equations for variables such as velocity, flow rate, and temperature fields are accomplished by combining perturbation and numerical techniques. In relation to the calendering process, the thickness of the exiting sheet is specifically explored. Furthermore, this study quantifies substantial engineering parameters such as roll-separating force, pressure distribution, and power transferal from the rolls to the fluid. The governing equations belong to three key dimensionless parameters, namely, the Brinkman number, which is a product of Eckert number and Prandtl number, the temperature-dependent consistency index μ, and a parameter η correlating to non-Newtonian behavior. The outcomes of this study are presented both graphically and in tabular form. It has been observed that a rise in the third-grade parameter decreases detachment point and sheet thickness due to increased material rigidity. Furthermore, established results in the literature regarding the calendering of Newtonian fluids are validated.

Keywords: calendaring, third-grade material, variable viscosity, rigid rolls, lubrication theory, numerical solutions, exact solutions

Nomenclature

H_0	half of the nip region
H/H_0	thickness of the coating
R (m)	roll radius
U	roll velocity $\left(\frac{m}{s}\right)$
ρ	fluid density $\left(\frac{\text{kg}}{\text{m}^3}\right)$
λ	dimensionless flow rate

1 Introduction

Calendering is a vital mechanical procedure in which a material, often in a semi-molten state, is passed through sets of heated rollers to achieve a sheet of desired thickness. The term calendering, derived from the Greek word "kylindros" meaning cylinder, refers to these combined rolls. The process significantly enhances the surface properties, reduces sheet thickness, and imparts special effects like a glaze or polish, which significantly affect the final product's aesthetics. There are many different ways by

* **Corresponding author: Fateh Ali,** College of Mathematics and System Sciences, Xinjiang University, Urumqi 830046, China, e-mail: fatehalirana@xju.edu.cn
* **Corresponding author: Basma Souayeh,** Department of Physics, College of Science, King Faisal university, P. O. Box 400, Al-Ahsa, 31982, Saudi Arabia; Laboratory of Fluid Mechanics, Physics Department, University of Tunis El Manar, Tunis, 2092, Tunisia, e-mail: bsouayeh@kfu.edu.sa
Muhammad Zahid: Department of Mathematics, COMSATS University Islamabad, Abbottabad Campus, 22060, Abbottabad, Pakistan
Muhammad Tahir Khan: Key Laboratory of Urban Rail Transit Intelligent Operation and Maintenance Technology & Equipment of Zhejiang Province, College of Engineering, Zhejiang Normal University, Jinhua 321004, China

which the calendaring process can be used in real life. Many industries, like those that make paper, textiles, plastics, and rubber, use calendaring methods. Calendering is an essential part of the paper business for improving paper products' surface finish, smoothness, and printability. It helps textile companies make materials with the right thickness, texture, and gloss. Calendering is used in the plastics industry to shape and laminate plastic sheets and films that are used for building materials, car parts, and packaging. Similarly, calendering is used to make sheets or coats for tires, conveyor belts, and seals, among other things, in the rubber industry. Overall, calendering is an important part of improving product quality, performance, and usefulness in many fields, which is why it is an essential part of modern manufacturing.

The technique has widespread application in various industries, especially in manufacturing paper, textiles, coated fabrics, and plastic films, to achieve a specified surface finish and texture. Edwin and Charles initially used this technique for shaping materials into films and sheets in the United States [1] in the 1830s. Ardichvili [2] later performed the first theoretical analysis of calendering, which was further extended for Newtonian and Bingham plastics by Gaskell [3]. The process has been subject to continuous improvements, with notable contributions from McKelvey [4] and Brazinsky *et al.* [5]. Alston and Astill [6] investigated hyperbolic tangent viscosity model fluids, while Middleman's [7] approximation solution focused on Maxwell fluid. Concurrently, Tokita and White [8] incorporated experimental observations on the milling of elastomers, and Sofou and Mitsoulis [9] provided numerical results for isothermal viscoelastic calendering sheets. Interestingly, Siddiqui *et al.* [10] observed the effect of magnetohydrodynamics (MHD) on the calendering of Newtonian material, proposing that magnetic fields serve as a pivotal parameter in modulating power transmission, separation force, and the divergence between attachment and detachment points. Siddiqui and his team [11] applied thermodynamically compatible models to third-grade fluid analysis in the calendering process, advancing our current understanding of this procedure. Calendering, as a finishing operation in the papermaking industry, has been used to enhance the smoothness and gloss of final paper products [12]. Their recent work has shed light on the surface morphology of calendered composite paper, providing valuable insights into the impact of calendering on fiber and paper. The research conducted by Zahid [12,13] highlighted the importance of calendering in achieving a smoother surface and enhancing the overall quality of paper products. Calendering dates back centuries and has been an important process in various industries. Research on the impact of various parameters, such as MHD, heat transfer, and other factors, on non-Newtonian fluid and nanofluids across different geometries has garnered significant attention in recent years due to its potential applications in various fields including engineering, biomedicine, and renewable energy [14–18]. The analysis of dimensionless parameters on different flow fields, conveyed through comprehensive graphs and tables, reveals a profound understanding. Through systematic variation and graphical representation, the study elucidates the significant impact of each parameter on key quantities of interest.

Third-grade fluids are recognized as a significant class of non-Newtonian materials. Among noteworthy research areas is the flow of non-Newtonian material due to counter-rotating rolls, considering its widespread applications in diversified industrial sectors like polymer film rolling and metal sheet extrusion. Numerous studies have been conducted on third-grade fluid, recognizing its pragmatic implications in contemporary science. Fosdick and Rajagopal [19] have crucially explored the stability of third-grade material. Meanwhile, other researchers [20] utilized numerical results and the finite-difference scheme to investigate the impact of fluctuating viscosity on third-grade material in a pipe. Further work by Abbasbandy *et al.* [21] employed numerical solutions to assess flows between two permeable walls of third-grade material. Yürüsoy [22] analyzed similarity solutions concerning third-grade material for specific channel coordinate systems. Ogunsola and Peter [23] conducted research on the effect of radiation and Arrhenius reaction on the flow of third-grade material. Adding to this, Akinshilo and Sobamowo [24] evaluated third-grade material's functionality as blood using gold nanoparticles. Aksoy and Pakdemirli [25] leveraged the perturbation solution in studying the third-grade material across diverse flow channels.

This theoretical research's vital aspect lies in the exploration of non-Newtonian material with variable viscosity. This is primarily because the customary Navier–Stokes theory becomes inadequate for describing complex rheological materials like polymer solutions, paints, and plastic films. Consequently, Massoudi and Christie [20] probed the influence of variable viscosity and the associated description of the third-grade fluid flow in a pipe. Based on this concept, Pakdemirli and Yilbas [26,27] worked on the closed-form solution using a perturbation method, determining the entropy generation for both Vogel and constant's model of viscosities. Jayeoba and Okoya [28] presented the analytical approximate solution to determine the temperature fields for the steady flow of a third-grade fluid in a pipe with models of viscosities, including a heat generation term for the no-slip boundary condition. Ali *et al.* [29] studied an Eyring-Powell fluid under the effects of temperature-dependent viscosity cases in a pipe. They first convert their dimensional forms of momentum and energy equations with boundary

conditions into non-dimensional form, and then discuss Reynolds and Vogel models for both momentum and energy equations. In their research work, they solved their equations with the help of both perturbation and numerical methods that match well. Yurusoy [22] presented the heat transfer effects of third-grade fluid between two concentric cylinders. During his study, he considered that the fluid temperature is lower than the pipe temperature. He calculated the solution by using the perturbation technique and discussed the Reynolds model. Makinde [30] studied the flow of thin films of Newtonian fluid with temperature-dependent viscosity down an inclined plate and obtained approximate analytical solutions using the perturbation method. Tshehla [31] investigated the flow of Newtonian fluid with temperature-dependent viscosity on an inclined plane with a free surface, solving the resulting system of coupled ordinary differential equations using the perturbation and Runge-Kutta numerical methods. In all such investigations, calendering with variable viscosity has not been considered [32]. The reader is encouraged to explore the provided references for a more comprehensive understanding of the topic [33].

This research provides a comprehensive theoretical exploration of the calendering procedure as applied to third-grade fluid. It delves intensely into the complex dynamics influenced by temperature variations as the fluid passes among two counter-rotating heated rolls. Notably, it addresses the unique challenges third-grade fluid encounters by emphasizing the impact of temperature-dependent viscosity, accurately captured through Reynold's model. The study innovatively employs the Lubrication approximation theory (LAT) to simplify the mass, momentum, and energy balance equations. The investigation of critical variables such as velocity, flow rate, and temperature fields was done using the perturbation method. Furthermore, the study quantifies essential engineering parameters such as roll-separating force, pressure distribution, and power transfer from rolls to the fluid, offering practical applications and refining the calendering process for third-grade fluid. This approach underscores the significance and innovation of calendering for such materials, contributing to advancements in both theoretical understanding and practical applications within relevant industries.

To the best of our knowledge, calendering a third-grade fluid with variable viscosity represents a novel advancement in the field, as no such study has been reported in existing literature.

2 Basic equations

The basic equations of the conservation of mass, conservation of momentum, and conservation of energy governing the flow of an incompressible, non-isothermal third-grade fluid in the absence of body forces are [34,35] as follows:

$$\nabla\cdot\mathbf{V} = 0, \tag{1}$$

$$\rho\frac{\mathrm{D}\mathbf{V}}{\mathrm{D}t} = \nabla\cdot\tau - \nabla p, \tag{2}$$

$$\rho C_{\mathrm{p}}\frac{\mathrm{D}\theta}{\mathrm{D}t} = \kappa\nabla^2\theta + \tau\cdot\nabla\mathbf{V}, \tag{3}$$

where $\mathbf{V}$ is the velocity field, ρ is the constant density, τ is the extra stress tensor, p is the material pressure, θ is the temperature, κ is the thermal conductivity, C_{p} is the specific heat, and $\frac{\mathrm{D}}{\mathrm{D}t}$ denotes the material time derivative, which is

$$\frac{\mathrm{D}(\cdot)}{\mathrm{D}t} = (\mathbf{V}\cdot\nabla)(\cdot) + \frac{\partial(\cdot)}{\partial t}. \tag{4}$$

The stress-constitutive relation τ for third-grade [36] material is given by

$$\tau = \mu A_1 + \alpha_1 A_2 + \alpha_2 A_1^2 + \beta(\mathrm{tr}A_1^2)A_1, \tag{5}$$

where $\mu(\theta)$ denotes the coefficient of viscosity and $\alpha_1(\theta)$, $\alpha_2(\theta)$, β are the material moduli, usually referred to as normal stress coefficients. However, the term β can be determined if the relationship between the stress and the Rivlin–Ericksen tensor of the fluid is known. The Rivlin–Ericksen tensor $\mathbf{A}_1$ and $\mathbf{A}_2$ are defined as

$$\mathbf{A}_1 = \nabla\mathbf{V} + (\nabla\mathbf{V})^*, \tag{6}$$

$$\mathbf{A}_n = \frac{D}{Dt}(\mathbf{A}_{n-1}) + \mathbf{A}_{n-1}(\nabla\mathbf{V}) + \mathbf{A}_{n-1}(\nabla\mathbf{V})^*, \quad n = 2, 3, \ldots \tag{7}$$

where ∇ is the gradient operator and * represents the transpose of a matrix. If all the coefficients except μ are set equal to zero, then the above model reduces to the classical linearly viscous model.

The Reynold viscosity model is exploited to represent the fluctuation of viscosity corresponding to the temperature. While the variables of the third-grade fluid could be temperature-dependent, they are, for simplicity in this context, regarded as constant. The definition of the Reynold model of viscosity is $\mu = \exp(-M\theta)$. Using the Maclaurin series, this expression can be written as

$$\mu = 1 - M\theta + O(\theta^2), \tag{8}$$

where M is a viscosity variation parameter and corresponds to a constant viscosity case if $M = 0$.

3 Formulation of the problem

Consider the two-dimensional, steady, and isothermal flow of a third-grade material, considered incompressible. To generate a sheet, the substance is permitted to be dragged through two counter-rotating rolls operating at identical angular velocities $U = \omega R$. The physical model under study is shown in Figure 1, where $2H_0$ is the smallest gap between the rollers, $x$and$y$ represents the material movement direction and gap-wise direction, respectively. Given the substantial disparity between the curved channel length created by the rollers and the gap at the nip, *i.e.*, $H_0 \ll R$, it is reasonable to be considered as two-dimensional flow.

$$V = [u(x, y), v(x, y)]. \tag{9}$$

Given the symmetric nature of the presented physical model, only the upper half of the physical model requires consideration. When faced with a complex physical system, scientists and engineers frequently simplify the mathematically determined model to provide an approximation that can be useful. The purpose of this process is to generate an approximation. A solid understanding of the physical system and a full comprehension of the various dimensions of the fluxes, forces, velocities, and other components that are involved in the problem is necessary for the successful implementation of simplifications. We form these simplifications by considering the more significant terms in the governing equations and disregarding the less significant ones. Since there is only a small amount of roll separation in the nip region, we will start with the LAT argument. The LAT, which posits that the most significant dynamic events occur predominantly in the nip-region, sets the stage for analysis. In this region, which spans distally to both sides by an order of x_0, the surfaces of the roll exhibit near-parallel. Now it is quite a reasonable physical situation to undertake that, $v \ll u$, and $\frac{\partial}{\partial x} \ll \frac{\partial}{\partial y}$. The material progresses in the x-direction, and the velocity in the y-direction is negligible. Then, Eq. (9) implies that $\frac{\partial u}{\partial x} = 0$, which means that $u = u(y)$. Hence, the velocity profile and temperature field can be of the form, $\mathbf{V} = [u(y), 0, 0]$, $\theta = \theta(y)$, and $u = u(y)$. Thus, the conservation of mass as defined in Eq. (1) is identically satisfied, the acceleration part $\frac{\mathrm{D}\mathbf{V}}{\mathrm{D}t}$ in the momentum equation is reduced to $\mathrm{div}\tau - \nabla p = 0$. This leads Eq. (2) in component form as

$$\frac{\mathrm{d}\tau_{xy}}{\mathrm{d}y} - \frac{\partial p}{\partial x} = 0, \tag{10}$$

$$\frac{\mathrm{d}\tau_{yy}}{\mathrm{d}y} - \frac{\partial p}{\partial y} = 0, \tag{11}$$

where

$$\tau_{xy} = \mu\frac{\mathrm{d}u}{\mathrm{d}y} + 2\beta\left(\frac{\mathrm{d}u}{dy}\right)^3 \tag{12}$$

and $\tau_{yy} = (2\alpha_1 + \alpha_2)\left(\frac{\mathrm{d}u}{\mathrm{d}y}\right)^2$.

Generalized pressure P can be introduced as

$$P = p - (2\alpha_1 + \alpha_2)\left(\frac{\mathrm{d}u}{\mathrm{d}y}\right)^2. \tag{13}$$

Using Eqs. (12) and (13) in Eqs. (10) and (11), we obtain the following momentum and energy equations:

$$\frac{\mathrm{d}}{\mathrm{d}y}\left(\mu\frac{\mathrm{d}u}{\mathrm{d}y}\right) + 6\beta\left(\frac{\mathrm{d}u}{\mathrm{d}y}\right)^2\frac{\mathrm{d}^2u}{\mathrm{d}y} = \frac{\partial P}{\partial x}, \tag{14}$$

$$\frac{\partial P}{\partial y} = 0, \tag{15}$$

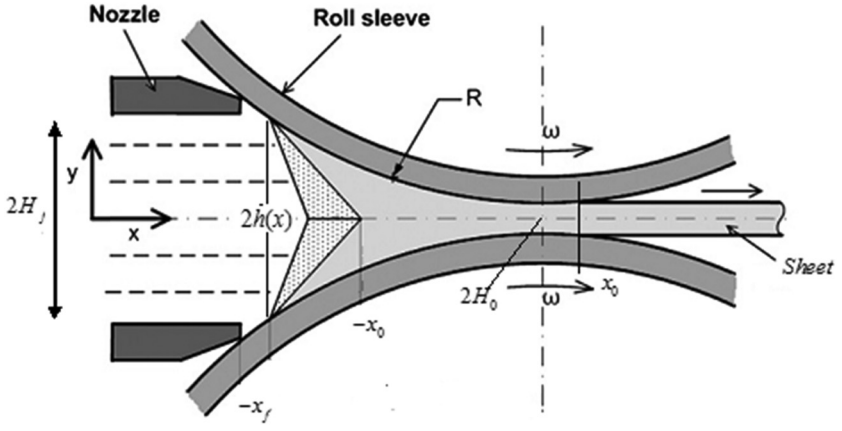

Figure 1: Mathematical illustration of the physical model under study.

Eq. (15) shows that $P = P(x)$, so Eq. (14) becomes

$$\frac{\mathrm{d}}{\mathrm{d}y}\left(\mu\frac{\mathrm{d}u}{\mathrm{d}y}\right) + 6\beta\left(\frac{\mathrm{d}u}{\mathrm{d}y}\right)^2\frac{\mathrm{d}^2u}{\mathrm{d}y} = \frac{\mathrm{d}P}{\mathrm{d}x}, \tag{16}$$

$$\kappa\frac{\mathrm{d}^2\theta}{\mathrm{d}y^2} + \mu\left(\frac{\mathrm{d}u}{\mathrm{d}y}\right)^2 + 2\beta\left(\frac{\mathrm{d}u}{\mathrm{d}y}\right)^4 = 0. \tag{17}$$

If both the rolls are identical and rotating with the same speed U, then the appropriate boundary conditions are

$$\left.\begin{aligned} &\text{at } y = h(x),\ u = U,\ \theta = \theta_0,\\ &\text{at } y = 0,\ \frac{\mathrm{d}u}{\mathrm{d}y} = 0,\ \frac{\mathrm{d}\theta}{\mathrm{d}y} = 0. \end{aligned}\right\} \tag{18}$$

where $h(x)$ represents the y-distance taken from the line of symmetry to the surface of the roll, *i.e.*,

$$h(x) = H_0 + R - (R^2 - x^2)^{\frac{1}{2}}. \tag{19}$$

By restricting the analysis to the values of x in such a way that $x \ll R$, we get a good approximation to $h(x)$ given as

$$h(x) = H_0\left(1 + \frac{x^2}{2H_0R}\right). \tag{20}$$

3.1 Dimensionless equations

Now define the following dimensionless variables [7]:

$$\begin{aligned} \bar{x} &= \frac{x}{\sqrt{RH_0}}, \bar{y} = \frac{y}{H_0}, \bar{u} = \frac{u}{U}, \bar{p} = \frac{pH_0^{3/2}}{\mu_0 UR^{1/2}}, \bar{\mu} = \frac{\mu}{\mu_0},\\ \bar{\theta} &= \frac{\theta - \theta_0}{\theta_1 - \theta_0}, \quad \bar{h}(\bar{x}) = \frac{h(x)}{H_0}. \end{aligned} \tag{21}$$

The dimensionless form of governing equations after ignoring the bar (−) sign are as follows:

$$\frac{\mathrm{d}}{\mathrm{d}y}\left(\mu\frac{\mathrm{d}u}{\mathrm{d}y}\right) + 6\eta\left(\frac{\mathrm{d}u}{\mathrm{d}y}\right)^2\frac{\mathrm{d}^2u}{\mathrm{d}y} = \frac{\mathrm{d}P}{\mathrm{d}x}, \tag{22}$$

$$\frac{\mathrm{d}^2\theta}{\mathrm{d}y^2} + \mu\omega\left(\frac{\mathrm{d}u}{\mathrm{d}y}\right)^2 + 2\eta\omega\left(\frac{\mathrm{d}u}{\mathrm{d}y}\right)^4 = 0. \tag{23}$$

The constants η and ω are given by

$$\begin{aligned} \eta &= \frac{\beta}{\mu_0}\left(\frac{U}{H_0}\right)^2, \quad \omega = \frac{\mu_0U^2}{\kappa(\theta_1 - \theta_0)} = \frac{\mu_0 c_\mathrm{p}}{\kappa} \times \frac{U^2}{c_\mathrm{p}(\theta_1 - \theta_0)}\\ &= \mathrm{PrEc}, \end{aligned} \tag{24}$$

where ω is the Brinkman number, that represents the ratio of viscous to inertial forces in a fluid flow system. It is defined as the product of Prandtl number Pr and Eckert number Ec, and the dimensionless boundary conditions [7] for the above system are

$$\left.\begin{aligned} &\text{at } y = h(x), u = 1, \theta = 1,\\ &\text{at } y = 0, \frac{\mathrm{d}u}{\mathrm{d}y} = 0, \frac{\mathrm{d}\theta}{\mathrm{d}y} = 0. \end{aligned}\right\} \tag{25}$$

The volumetric flow rate in dimensionless form, $\bar{Q}$ per unit width, may be defined as

$$\bar{Q} = \int_0^{h(x)} u\mathrm{d}y, \tag{26}$$

where the dimensional flow rate Q, per unit width, can be related by $\bar{Q} = \frac{Q}{2UH_0}$.

4 Solution of the problem

In this section, velocity profiles and temperature distributions are computed by using regular perturbation theory. The regular perturbation method is a critical tool for approximating solutions to differential equations, particularly valuable when the exact solutions cannot be explicitly stated or are tough to compute. It is a commonly used analytical approach in mathematics and engineering. The perturbation technique assumes a small parameter, often denoted as ε, that perturbs a system from a state where the solution is known. The solution is then expanded as a power series in terms of ε. Each term in the series is an order of magnitude smaller than the preceding term, comprising of the “unperturbed” solution and successive “corrections.” After substituting the power series into the differential equation, one matches the powers of ε to derive an associated sequence of simpler equations. The desired approximated solution is then acquired by solving these equations recursively. The method considerably simplifies the analytical solving process, making it a valuable tool for solving complex differential equations. We can obtain approximate solutions by selecting $\eta = \varepsilon\gamma$ and $M = \varepsilon m$, where ε is the perturbation parameter, *i.e.*, a small quantity. The approximate velocity profile, pressure gradient, flow rate, and temperature distribution can be taken as

$$u = u_0 + \varepsilon u_1 + O(\varepsilon^2), \tag{27}$$

$$\frac{\mathrm{d}p}{\mathrm{d}x} = \frac{\mathrm{d}p_0}{\mathrm{d}x} + \varepsilon\frac{\mathrm{d}p_1}{\mathrm{d}x} + O(\varepsilon^2), \tag{28}$$

$$\theta = \theta_0 + \varepsilon\theta_1 + O(\varepsilon^2), \tag{29}$$

$$\lambda = \lambda_0 + \varepsilon\lambda_1 + O(\varepsilon^2). \tag{30}$$

Viscosity and its derivative from Eq. (8) lead approximately as follows

$$\mu \cong 1 - \varepsilon m\theta, \quad \frac{d\mu}{dy} \cong -\varepsilon m\frac{d\theta}{dy}. \tag{31}$$

Substituting Eqs. (27)–(31) in Eqs. (22) and (23), one can yield the system of differential equations, as shown in Sections 4.1 and 4.2.

4.1 System of order ε^0 and their solution

The zero-order boundary value problem [7] is

$$\frac{d^2u_0}{dy^2} = \frac{dp_0}{dx}, \tag{32}$$

$$\frac{d^2\theta_0}{dy^2} = -\omega\left(\frac{du_0}{dy}\right)^2, \tag{33}$$

subject to boundary conditions

$$\left.\begin{aligned} &\text{at } y = h(x),\ u_0 = 1,\ \theta_0 = 1,\\ &\text{at } y = 0,\ \frac{du_0}{dy} = 0,\ \frac{d\theta_0}{dy} = 0. \end{aligned}\right\} \tag{34}$$

Solving for the first order, we obtain the following solutions that satisfy the boundary conditions

$$u_0 = 1 + \frac{1}{2}\frac{dp_0}{dx}(y^2 - h^2), \tag{35}$$

$$\frac{dP_0}{dx} = \frac{-3(\lambda_0^2 - x^2)}{h^3}, \tag{36}$$

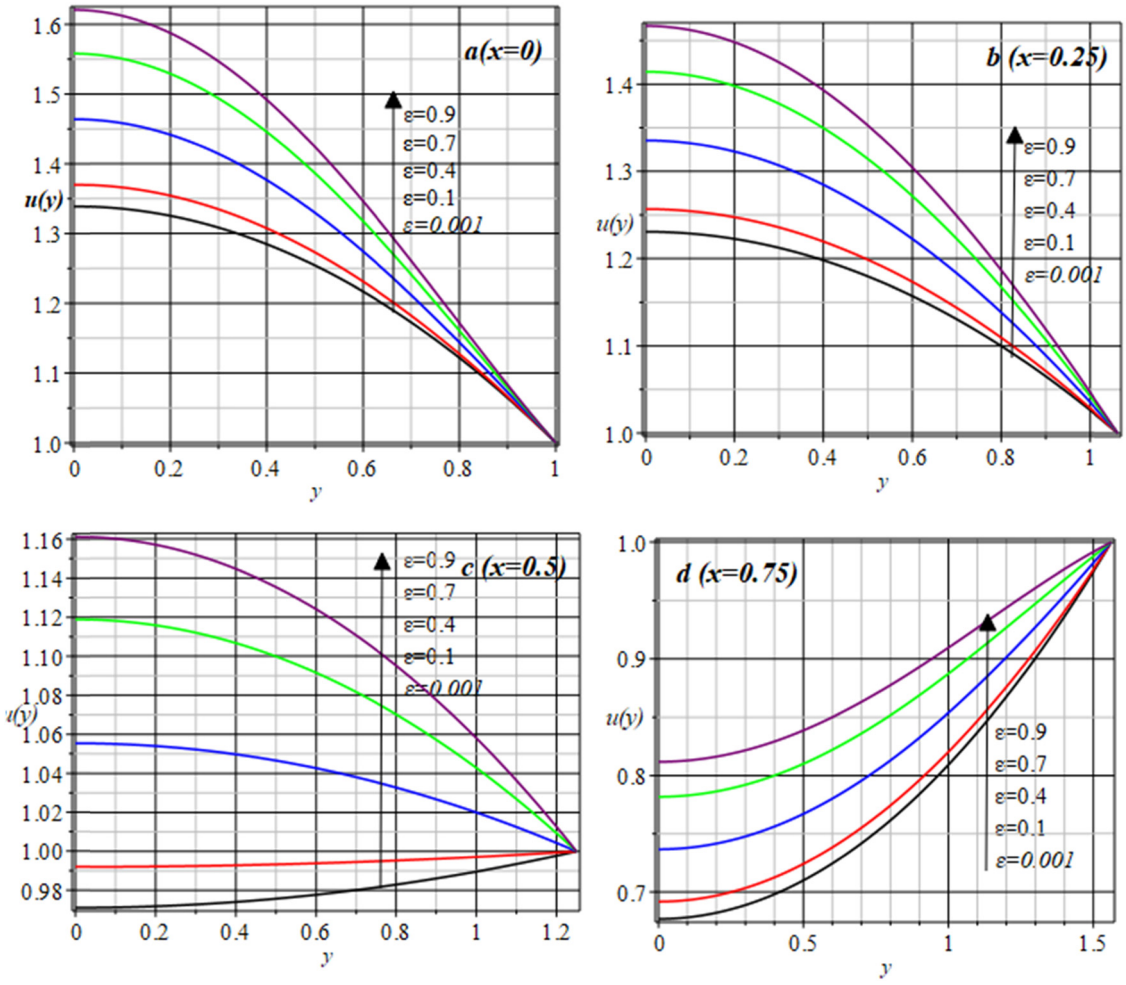

Figure 2: Effect of perturbation parameter on velocity distribution at four different positions of calendaring process at $m = 1.5$, $\gamma = 1.5$, $\omega = 1.5$, $\lambda_0 = 0.4751$. (a) $x = 0$, (b) $x = 0.25$, (c) $x = 0.5$, and (d) $x = 0.75$.

$$Q_0 = h - \frac{h^3}{3}\frac{dP_0}{dx}, \tag{37}$$

$$\theta_0 = \frac{3\omega(\lambda_0^2 - x^2)^2}{4h^2}\left[1 - \left(\frac{y}{h}\right)^4\right] + 1. \tag{38}$$

The pressure at the separation point may be found by the first integration of Eq. (36), using ($x = -\infty$) we get

$$P_0 = \frac{3}{8}\left[\left(\frac{x^2(1 - 3\lambda_0^2) - 1 - 5\lambda_0^2}{(1 + x^2)^2}\right)x + (1 - 3\lambda_0^2)(\tan^{-1}x - \tan^{-1}\lambda_0) + \left(\frac{3\lambda_0^2 + 1}{1 + \lambda_0^2}\right)\lambda_0\right]. \tag{39}$$

The most basic dynamic model of the separation region stems from the declaration that the fluid divides at the point where $u_0 = 0$ and $P_0 = 0$ subsequently. In light of this, the above equation transposes to a transcendental equation in the λ_0 variable. A solution for this could be approximated using a numerical technique known as the modified Regula falsi method. The estimated value for the zero-order detachment point came out to be $\lambda_0 = 0.4751$, which has been obtained by setting a predefined accuracy of 10^{-10}.

4.2 System of order ε^1 and their solution

The first-order system with appropriate boundary conditions is

$$\frac{d^2u_1}{dy^2} - m\theta_0\frac{d^2u_0}{dy^2} - m\frac{du_0}{dy}\frac{d\theta_0}{dy} + 6\gamma\left(\frac{du_0}{dy}\right)^2\left(\frac{d^2u_0}{dy^2}\right) = \frac{dp_1}{dx}, \tag{40}$$

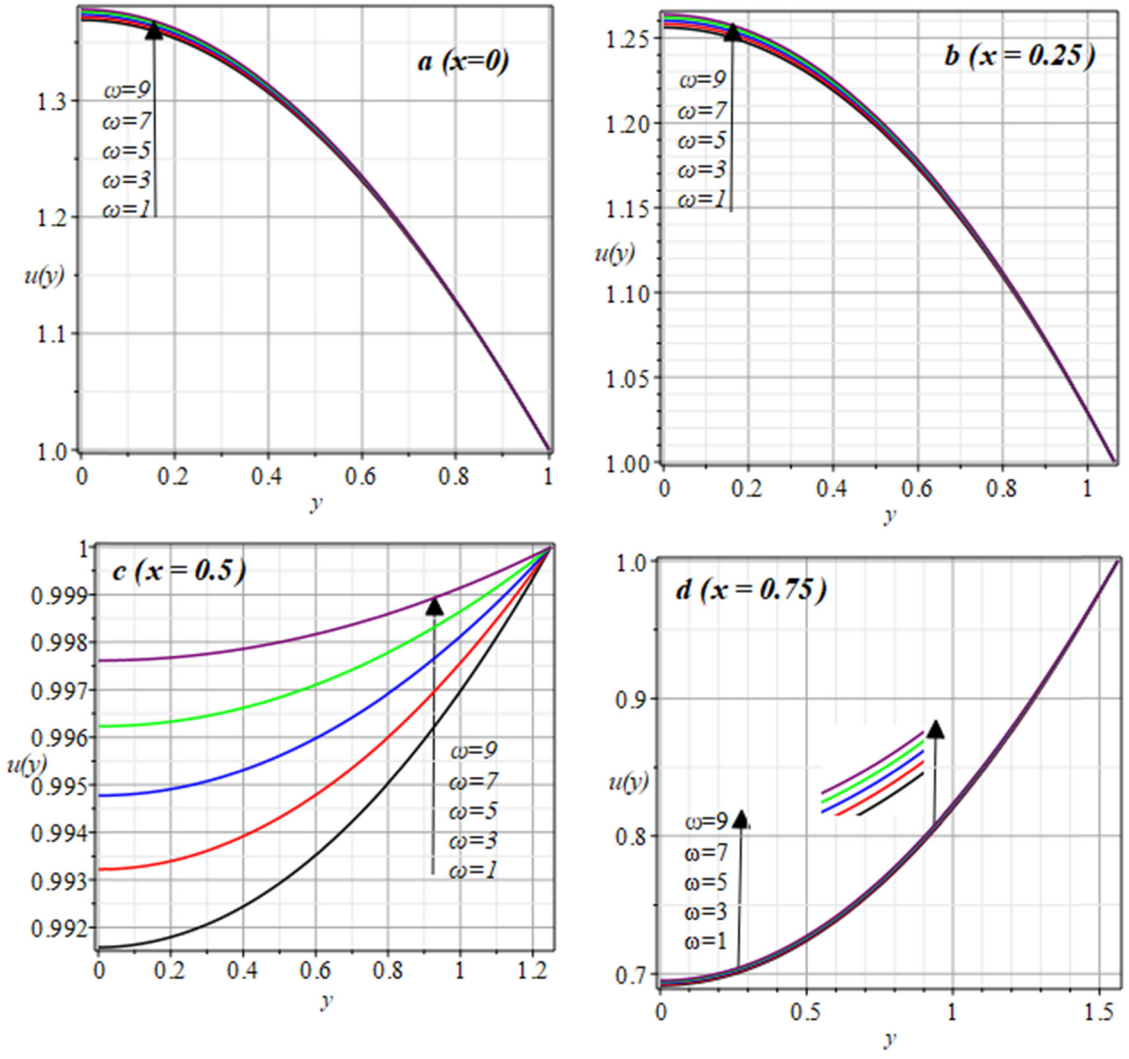

Figure 3: Effect of Brinkman number on velocity distribution at four different positions of calendaring process at $m = 1.5$, $\gamma = 1.5$, $\varepsilon = 0.1$, $\lambda_0 = 0.4751$. (a) $x = 0$, (b) $x = 0.25$, (c) $x = 0.5$, and (d) $x = 0.75$.

$$\frac{d^2\theta_1}{dy^2} - m\omega\theta_0\left(\frac{du_0}{dy}\right)^2 + 2\omega\frac{du_0}{dy}\frac{du_1}{dy} + 2\gamma\omega\left(\frac{du_0}{dy}\right)^4 = 0, \quad (41)$$

$$\left.\begin{aligned} &\text{at } y = h(x), u_1 = 0, \theta_1 = 0, \\ &\text{at } y = 0, \frac{du_1}{dy} = 0, \frac{d\theta_1}{dy} = 0. \end{aligned}\right\} \quad (42)$$

Solving the above system of order ε^1, we finally obtain the following solutions

$$u_1 = \frac{3}{4h^9}(\lambda_0^2 - x^2)\left[2h^6m(h^2 - y^2) + (\lambda_0^2 - x^2)^2\left\{\frac{\omega m}{2}(y^6 + 2h^6) - \frac{3}{2}\omega h^4 m y^2 - 18\gamma(h^4 - y^4)\right\}\right] - \frac{1}{2}\frac{dP_1}{dx}(h^2 - y^2), \quad (43)$$

$$\theta_1(y) = \frac{3\omega}{4h^{12}}(\lambda_0^2 - x^2)^4\left[\frac{\omega m}{56}\{(3y^4 - 3h^4)(3y^4 - 11h^4)\} + \frac{36}{5}\gamma(y^6 - h^6)\right] - \frac{3\omega m}{4h^6}(\lambda_0^2 - x^2)^2(y^4 - h^4) + \frac{\omega}{2h^3}\frac{dP_1}{dx}(\lambda_0^2 - x^2)(y^4 - h^4), \quad (44)$$

$$Q_1 = \frac{3}{h^9}(\lambda_0^2 - x^2)\left\{\frac{1}{3}mh^9 + \frac{1}{7}\omega m h^7(\lambda_0^2 - x^2)^2 - \frac{18}{5}\gamma h^5(\lambda_0^2 - x^2)^2\right\} - \frac{h^3}{3}\frac{dP_1}{dx}, \quad (45)$$

$$\frac{dp_1}{dx} = \frac{9}{h^{12}}(\lambda_0^2 - x_0^2)\left[\frac{1}{3}mh^9 + \frac{1}{7}\omega m h^7(\lambda_0^2 - x_0^2)^2 - \frac{18}{5}\gamma h^5(\lambda_0^2 - x_0^2)^2\right] - \frac{6\lambda_0\lambda_1}{h^3}. \quad (46)$$

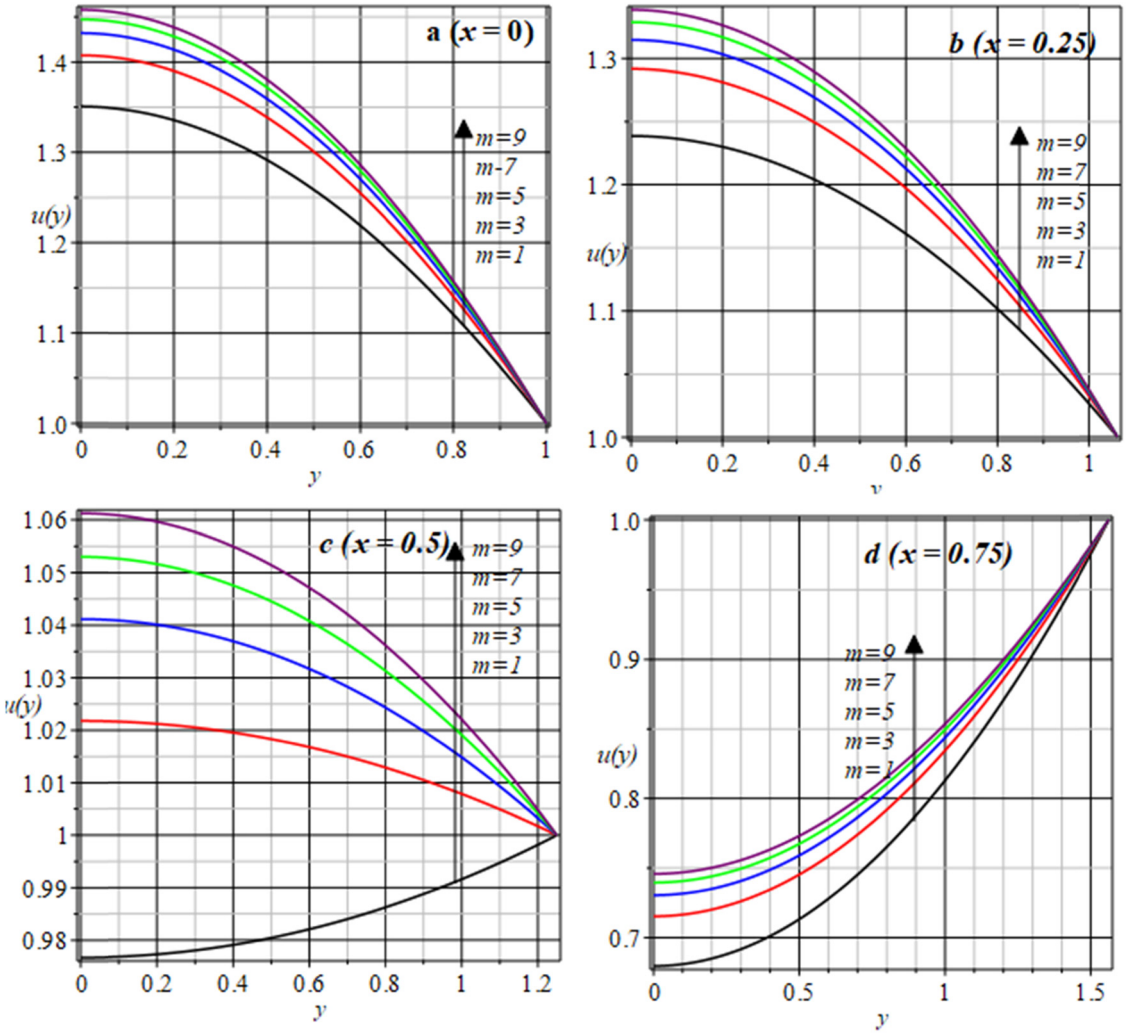

Figure 4: Effect of viscosity variation parameter on velocity distribution at four different positions of calendering process at $\varepsilon = 0.1$, $\gamma = 1.5$, $\omega = 1.5$, $\lambda_0 = 0.4751$. (a) $x = 0$, (b) $x = 0.25$, (c) $x = 0.5$, and (d) $x = 0.75$.

After using zero-order and first-order solutions in Eqs. (27)–(31), the series solution in terms of small parameter ε can be obtained. The graphical representation of these graphs are shown in Figures 2–8.

5 Operating parameters

When the velocity, pressure gradient, and pressure distribution are formed, then we can calculate all other engineering quantities. The emerging variables that are under consideration from the engineering point of view are computed as follows.

5.1 Roll-separating force

By making use of the dimensionless parameters as defined in Eq. (14), the total force involved to separate the fluid in dimensionless form after dropping the bar sign becomes

$$\frac{F}{W} = \int_{-\infty}^{\lambda} p(x)\mathrm{d}x. \tag{47}$$

5.2 Power

Using non-dimensional variables, *i.e.*, $\bar{P}_{\mathrm{W}} = \frac{P_{\mathrm{W}}}{\eta_0 W U^2}$ and $\overline{\tau}_{xy} = \frac{H_0 \tau_{xy}}{\eta_0 U}$ for power, the dimensionless form (on dropping bar sign), and putting $\bar{y} = h$, we obtain

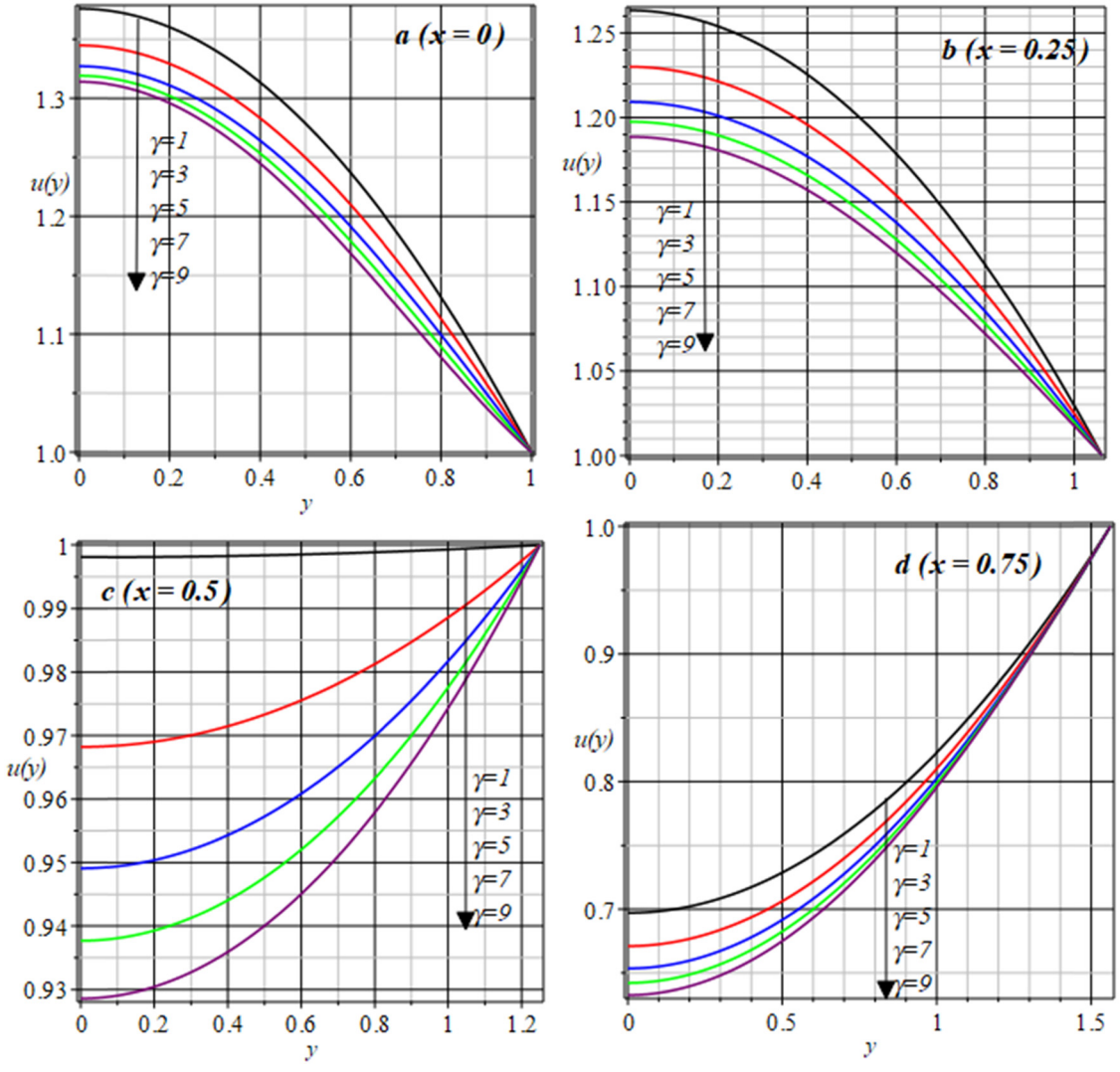

Figure 5: Effect of third-grade parameter on velocity distribution at four different positions of calendering process at $\varepsilon = 0.1$, $m = 1.5$, $\omega = 1.5$, $\lambda_0 = 0.4751$. (a) $x = 0$, (b) $x = 0.25$, (c) $x = 0.5$, and (d) $x = 0.75$.

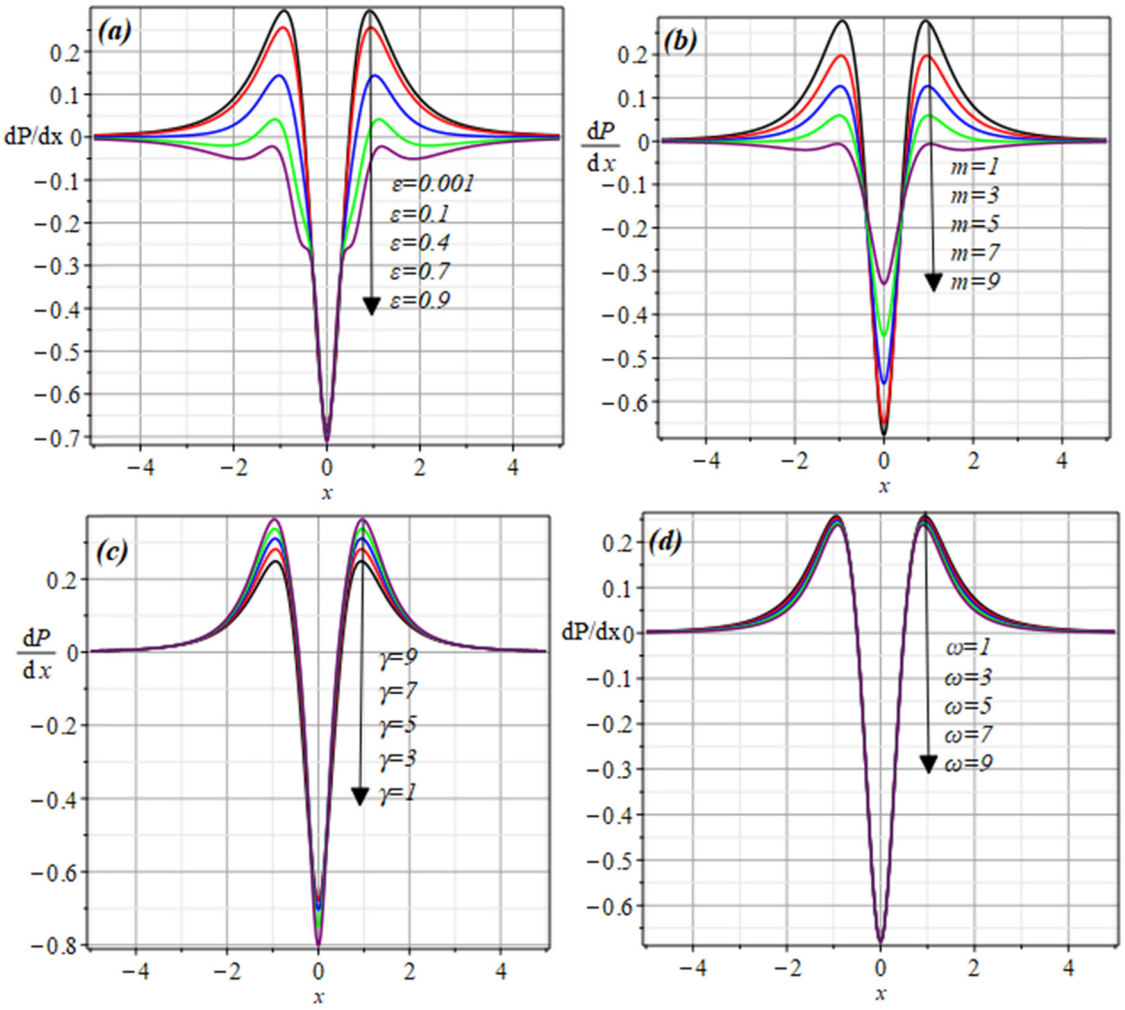

Figure 6: Influence of emerging parameters on pressure-gradient distribution.

$$P = \int_{-\infty}^{\lambda} \tau_{xy}(x, h)\mathrm{d}x, \tag{48}$$

where τ_{xy} is the dimensionless stress tensor defined by

$$\tau_{xy} = \frac{\partial u}{\partial y} + \beta\left(\frac{\partial u}{\partial y}\right)^3. \tag{49}$$

6 Results and discussion

The presented study discusses an interpretation of the calendering process for an incompressible viscoelastic material. The numerical exploration of varied engineering parameters concerning the viscoelastic material in the course of the calendering process is delineated in Tables 1–4. Figures 2–8 graphically illustrate the impact of emerging parameters on aspects such as velocity distribution, pressure gradient distribution, pressure distribution, and temperature. Table 1 presents the ramifications of the perturbation parameter ε on various factors, including the detachment point λ, the thickness of the sheet, the force separating the roll, and the power input. It has been noted that with an increase in the perturbation parameter, there is an elevation in the detachment, sheet thickness, and roll-separating force, whereas power input from the roll to the material witnesses a decrease. The results found by Middleman [7] when $\varepsilon \to 0$ have been affirmed in this study. In Table 2, the effects of the viscosity parameter "m" are explored. It can be observed that with an upsurge in the coefficient of the viscosity parameter, the detachment point and sheet thickness experience an increase, while on the contrary, there is a decrease in both the power input and the roll-separating force. The outcomes of this research resonate with the findings of Siddiqui [16] when "$m = 0$" is considered as an extreme case of the study.

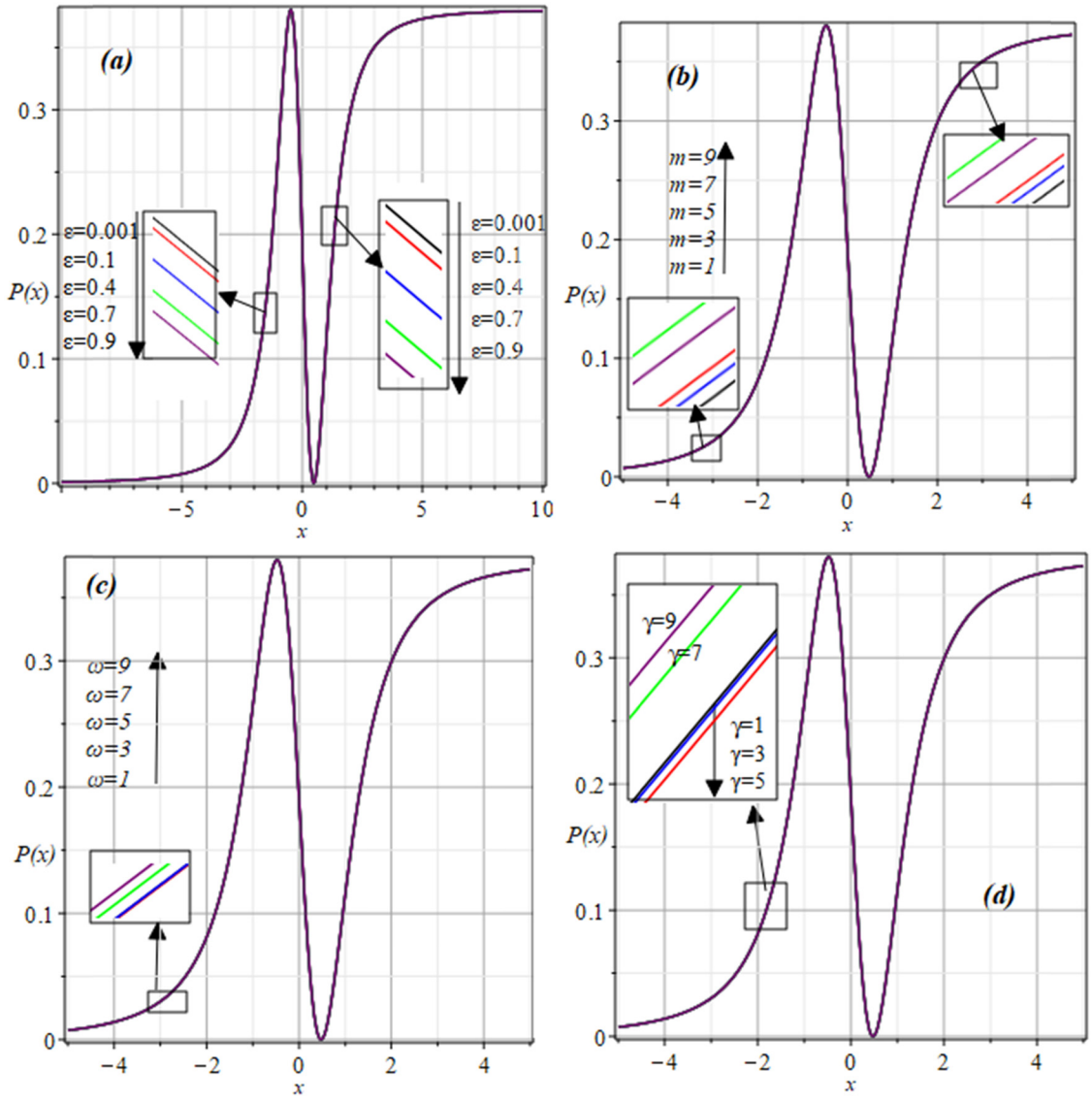

Figure 7: Influence of emerging parameters on pressure distribution.

This study presents numerical outcomes corresponding to several engineering parameters concerning the Brinkman number, as documented in Table 3. The Brinkman number, commonly employed in polymer processing, is associated with heat conduction transitioning from the roller wall to the material in flow. A surge in the Brinkman number causally relates to an increase in both the detachment point and sheet thickness, conversely observing a decrease in power input and roll-separating force. Of note is the fact that the detachment points approach 0.4751 as the Brinkman number continues to increase ($\omega \to \infty$).

Table 4 elucidates the variations occurring in the third-grade parameter and investigates its influence on various engineering parameters. Analyzing the collected data reveals that an escalation in the third-grade parameter corresponds to a decrease in both the detachment point and the sheet thickness. This outcome can be attributed to the fact that the rigidity of the material increases in proportion to the increase in the third-grade parameter. Notably, the third-grade parameter serves as a controlling parameter for all engineering quantities, with an emphasis on the sheet thickness. Additionally, fluctuating the third-grade parameter indicates an increment in the power input from the rolls, whereas there appears to be a decline in the roll-separating forces.

Figures 2–5 illustrate velocity at various stages in the calendering process, factoring in four distinct parameters. Figure 2 demonstrates explicitly how altering the perturbed parameter impacts the velocity distribution across various stages of the calendering recess. Fascinatingly, the figure shows that when the perturbed parameter increases,

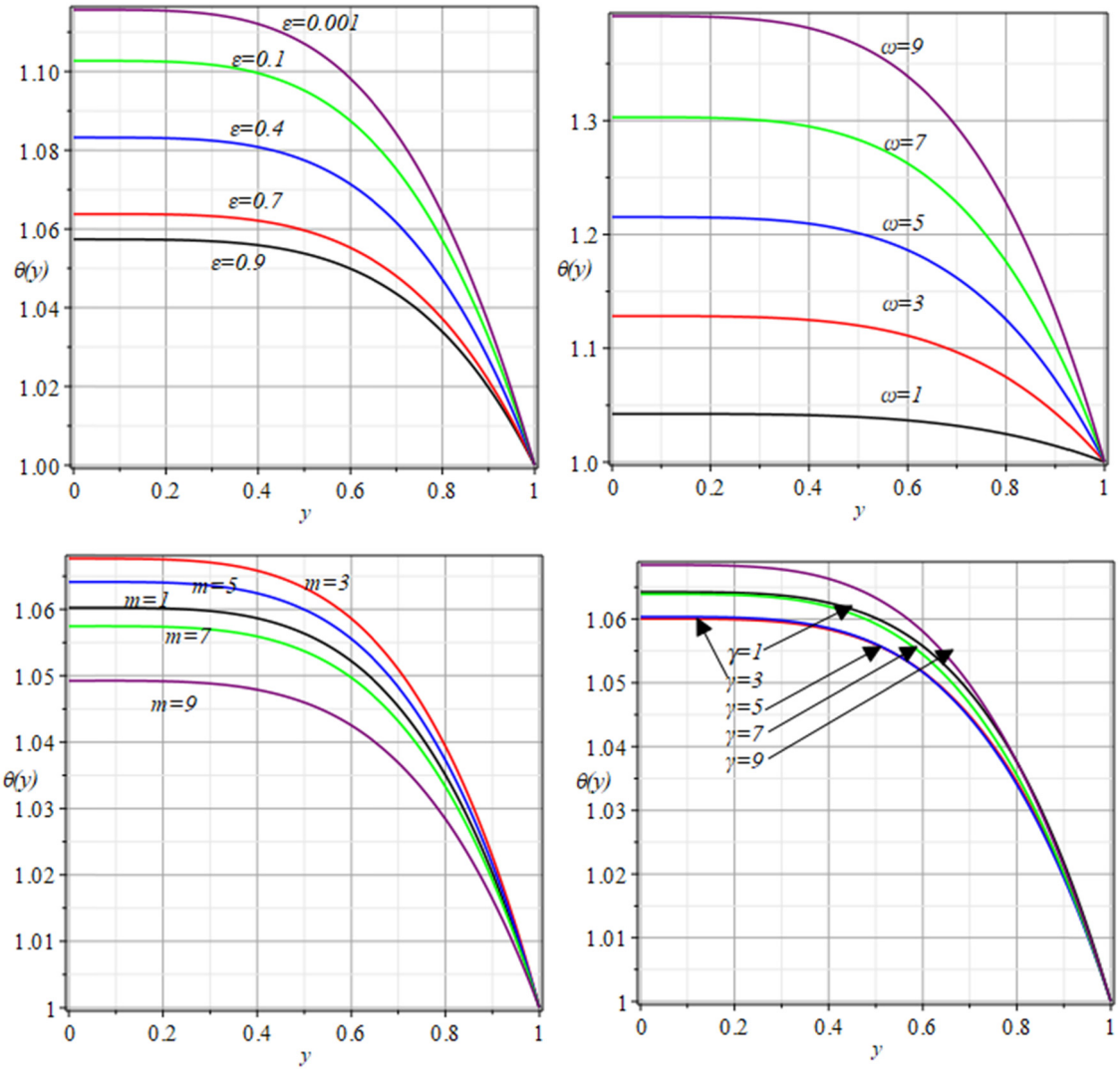

Figure 8: Influence of emerging parameters on temperature distribution.

Table 1: Influence of perturbation parameter on engineering quantities at $\omega = 1.5$, $m = 1.5$, $\gamma = 1.5$, $\lambda_0 = 0.4751$, $\lambda_1 = 0.1854$

ε	λ	H/H_0	P_w	F
0.001	0.4752	1.2258	1.6248	0.6061
0.004	0.4758	1.2263	1.6188	0.6062
0.007	0.4763	1.2268	1.6129	0.6063
0.01	0.4769	1.2274	1.6069	0.6063
0.04	0.4825	1.2328	1.5467	0.6070
0.07	0.4880	1.2381	1.4856	0.6078
0.1	0.4936	1.2436	1.4237	0.6085
0.4	0.5492	1.3016	0.7674	0.6163
0.7	0.6048	1.3657	0.0588	0.6253
0.9	0.6419	1.4120	−0.4393	0.6319

Table 2: Influence of viscosity variation parameter on engineering quantities at $\omega = 1.5$, $\gamma = 1.5$, $\varepsilon = 0.1$, $\lambda_0 = 0.4751$

m	λ_1	λ	H/H_0	P_w	F
1	0.0511	0.4802	1.2305	1.5139	0.6069
2	0.2980	0.5049	1.2549	1.3411	0.6088
3	0.4465	0.5197	1.2700	1.2029	0.6062
4	0.5440	0.5295	1.2803	1.0831	0.5980
5	0.6165	0.5367	1.2880	0.9724	0.5832
6	0.6736	0.5424	1.2941	0.8674	0.5619
7	0.7203	0.5471	1.2993	0.7663	0.5345
8	0.7594	0.5510	1.3036	0.6679	0.5014
9	0.7926	0.5543	1.3072	0.5719	0.4631
10	0.8213	0.5572	1.3104	0.4775	0.4197

Table 3: Influence of Brinkman number on engineering quantities at $\varepsilon = 0.1$, $\lambda_0 = 0.4751$, $m = 1.5$, $\gamma = 1.5$

ω	λ_1	λ	H/H_0	P_w	F
1	0.1817	0.4932	1.2432	1.4672	0.6085
2	0.1890	0.4940	1.2440	1.3804	0.6085
3	0.1961	0.4947	1.2447	1.2937	0.6085
4	0.2030	0.4954	1.2454	1.2073	0.6084
5	0.2097	0.4960	1.2460	1.1209	0.6084
6	0.2162	0.4967	1.2467	1.0347	0.6083
7	0.2225	0.4973	1.2473	0.9486	0.6083
8	0.2287	0.4979	1.2479	0.8626	0.6082
9	0.2346	0.4985	1.2485	0.7767	0.6082
10	0.2405	0.4991	1.2491	0.6909	0.6081

the velocity distribution rises. This outcome thus leads to the inference that it is possible to manipulate the material's speed at different stages in the shaping process by adjusting this specific parameter.

Figure 3 displays the influence of the Brinkman number on velocity distribution at different positions. In this case, an enhancement in the Brinkman number coincides with an increase in velocity distribution, the effect of which is most apparent at $x = 0.5$ position. Since, the Brinkman number characterizes the ratio of viscous forces to inertial forces, with the increase in the Brinkman number, the contribution of viscous forces becomes more dominant relative to inertial forces. This increased dominance of viscous forces results in more excellent resistance to fluid flow, leading to higher velocity. Therefore, as the Brinkman number increases, the velocity distribution of fluid flow also increases. Next the impact of changes in the viscosity variation parameter is demonstrated in Figure 4. Here it becomes evident that an increase in this parameter also triggers a rise in velocity distribution. Physically, it means that viscosity is often temperature-dependent, especially for non-Newtonian fluids used in this analysis of calendering processes. By increasing the temperature of the fluid, its viscosity decreases, making it flow more easily. So, this decrease in viscosity makes it easier for the fluid to flow, resulting in higher velocity.

Table 4: Influence of third-grade parameter γ on engineering quantities at $\varepsilon = 0.1$, $\lambda_0 = 0.4751$, $m = 1.5$, $\omega = 1.5$

γ	λ_1	λ	H/H_0	P_w	F
1	0.2386	0.4989	1.2489	1.4110	0.6078
2	0.1181	0.4869	1.2370	1.4414	0.6085
3	−0.0232	0.4727	1.2234	1.4785	0.6053
4	−0.1218	0.4629	1.2142	1.5001	0.6012
5	−0.1910	0.4560	1.2079	1.5110	0.5980
6	−0.2452	0.4505	1.2029	1.5167	0.5952
7	−0.2910	0.4460	1.1989	1.5193	0.5927
8	−0.3322	0.4418	1.1951	1.5203	0.5900
9	−0.3706	0.4380	1.1918	1.5202	0.5870
10	−0.4079	0.4343	1.188	1.5198	0.5835

Finally, Figure 5 illustrates how velocity distribution fluctuates concerning modifications in the third-grade parameter. Upon investigation, we discovered that velocity distribution decreases when the third-grade parameter increases during the calendering process. This outcome hints that the fluid becomes more viscous as the third-grade parameter increases. It is important to note that the increased viscosity of the material as it propelled toward the detachment point can aid in swiftly forming the sheet.

Figure 6 provides an intriguing perspective on the pressure gradient as a function of x. It highlights its growth and peak just before the nip region, followed by a steady decline across different numerical values of emerging parameters. More specifically, it showcases that an escalation in these emerging parameters corresponds with a decrease in the pressure gradient distribution. For an even deeper understanding of this process, one can turn to Figure 7. This graph provides significant insights into the highest and lowest points of pressure distribution throughout the calendering gap. It also offers clear visualizations of the attachment and detachment points, a crucial feature for understanding the mechanics of the process.

Furthermore, this figure compares how pressure distribution reacts to individual parameter changes. Increases in both the perturbation and third-grade parameters result in an upswing in pressure distribution. Contrarily, the pressure distribution displays a contrasting behavior when changes proceed in the other two emerging parameters, demonstrating a decrease in value, as shown in Figure 7.

Figure 8 presents a thorough analysis of the impact produced by various emerging parameters on temperature distribution when both rolls undergo a heat process. The graphical representation of the said parameters clearly illustrates this relationship. In Figure 8a and b, the findings indicate a reduction in temperature distribution upon increasing the values of the perturbation parameter and the Brinkman number, respectively. As the Brinkman number increases, the dominance of viscous effects over inertial effects can lead to increased internal friction and reduced convective heat transfer within the fluid, ultimately decreasing temperature. These findings manifest the nuanced interactions within the system. However, the analysis portrays a more complex pattern for the viscosity variation parameter and, similarly, for the third-grade parameter. Figure 8c and d illustrates a mixed-type behavior.

This signals the presence of a non-linear interaction and possibly a more complex relationship between these specific parameters and the temperature distribution. These variations underline the multi-faceted nature of the system under examination.

7 Conclusion

In conclusion, this comprehensive study delved into the intricate aspects of heat transfer flow involving third-grade materials passing between two heated rolls with distinct temperature gradients. This research has unveiled critical insights by incorporating temperature-dependent viscosity using Reynold's model and the application of the LAT to simplify mass, momentum, and energy balance equations. The investigation focused on essential parameters governing the calendering process, presenting results through graphical representations and tabular summaries. The study has uncovered several crucial insights regarding the process. Notably, the impact of parameters such as the perturbation parameter, viscosity parameter, Brinkman number, and third-grade parameters on detachment point, sheet thickness, roll-separating force, and power input has been thoroughly investigated. We saw that as the perturbation parameter along with the detachment point, sheet thickness, and roll-separating force all increased while the power input decreased. Similarly, a higher viscosity parameter increases detachment point and sheet thickness but decreases power input and roll-separating force. Increasing the Brinkman number also raises the detachment point and sheet thickness but lowers power input and roll-separating force. Conversely, a rise in the third-grade parameter results in decreased detachment point and sheet thickness due to increased material rigidity. The study also looked at how perturbation, Brinkman number, and viscosity variation parameters affect the pressure gradient changes when emerging parameters change, with a focus on the points of attachment and detachment.

The findings from this study can be applied to optimize the calendering process in industries dealing with viscoelastic materials, such as polymer processing, textile manufacturing, and paper production. Understanding the influence of variable viscosity on sheet thickness, detachment points, and power input can lead to improved process efficiency and product quality.

The insights gained from quantifying engineering parameters can inform the design of calendering systems, helping engineers and researchers tailor process parameters to achieve desired material properties and performance characteristics.

Acknowledgments: This work was supported by the Deanship of Scientific Research, Vice Presidency for Graduate Studies and Scientific Research, King Faisal University, Saudi Arabia (Grant No. 6049) and the Talent Project of Tianchi Doctoral Program in Xinjiang Uyger Autonomous Region of China.

Funding information: This work was supported by the Deanship of Scientific Research, Vice Presidency for Graduate Studies and Scientific Research, King Faisal University, Saudi Arabia (Grant No. 6049) and the Talent Project of Tianchi Doctoral Program in Xinjiang Uyger Autonomous Region of China.

Author contributions: Muhammad Zahid: conceptualization, mathematical modeling, solution methodology, writing - original draft, and software; Fateh Ali: discussion, software, solution, and writing review - editing; Basma Souayeh: discussion, review - editing, English correction, and funding; and Muhammad Tahir Khan: review - editing and English correction. All authors have accepted responsibility for the entire content of this manuscript and approved its submission.

Conflict of interest: The authors state no conflicts of interest.

Data availability statement: All data generated or analyzed during this study are included in this published article.

References

[1] Osswald TA, Menges G. Materials science of polymers for engineers. Germany: Carl Hanser Verlag GmbH Co KG; 2012.
[2] Ardichvili G. An attempt at a rational determination of the ambering of calender rolls. Germany: Kautschuk; 1938.
[3] Gaskell R. The calendering of plastic materials. J Appl Mech. 1950; 17(3):334–6
[4] McKelvey JM. Processing P. New York: John Wiley & Sons. Inc; 1962.
[5] Brazinsky I, Cosway H, Valle Jr C, Jones RC, Story V. A theoretical study of liquid-film spread heights in the calendering of Newtonian and power law fluids. J Appl Polym Sci. 1970;14:2771–84.
[6] Alston Jr WW, Astill KN. An analysis for the calendering of non-Newtonian fluids. J Appl Polym Sci. 1973;17:3157–74.
[7] Middleman S. Fundamentals of polymer processing, New York, USA: Mcgraw-Hill; 1977.
[8] White JL, Tokita N. Elastomer processing and application of rheological fundamentals. J Appl Polym Sci. 1967;11:321–34.
[9] Sofou S, Mitsoulis E. Calendering of pseudoplastic and viscoplastic sheets of finite thickness. J Plastic Film Sheeting. 2004;20:185–222.
[10] Siddiqui A, Zahid M, Rana M, Haroon T. Effect of magnetohydrodynamics on Newtonian calendering. J Plastic Film Sheeting. 2013;29:347–64.
[11] Siddiqui A, Zahid M, Rana M, Haroon T. Calendering analysis of a third-order fluid. J Plastic Film Sheeting. 2014;30:345–68.

[12] Zhao Y, Shen Q, Duan Y, Wu S, Lei P, Yang L, et al. Wood fiber-reinforced polylactic acid sheets enabled by papermaking. BioResources. 2021;16:8258.
[13] Zahid M, Haroon T, Rana M, Siddiqui A. Roll coating analysis of a third grade fluid. J Plastic Film Sheeting. 2017;33:72–91.
[14] Ishtiaq B, Nadeem S, Abbas N. Theoretical study of two-dimensional unsteady Maxwell fluid flow over a vertical Riga plate under radiation effects. Sci Iran. 2022;29:3072–83.
[15] Abbas N, Nadeem S, Saleem A, Issakhov A, Abdel-Sattar M, Aly S. Analysis of non-Newtonian fluid with phase flow model. Sci Iran. 2021;28:3743–52.
[16] Ur Rehman A, Nadeem S, Abbas N, Mehmood R. Analytical view of magnetic hydrodynamic rotating flow of Barium Ferrite nanofluid with viscous dissipation. Sci Iran. 2020;27:3421–33.
[17] Narayana PS, Babu DH. Numerical study of MHD heat and mass transfer of a Jeffrey fluid over a stretching sheet with chemical reaction and thermal radiation. J Taiwan Inst Chem Eng. 2016;59:18–25.
[18] Harish Babu D, Satya Narayana P. Melting heat transfer and radiation effects on Jeffrey fluid flow over a continuously moving surface with a parallel free stream. J Appl Comput Mech. 2019;5:468–76.
[19] Fosdick R, Rajagopal K. Thermodynamics and stability of fluids of third grade. Proceedings of the Royal Society of London A Mathematical and Physical Sciences. Vol. 369; 1980. p. 351–77.
[20] Massoudi M, Christie I. Effects of variable viscosity and viscous dissipation on the flow of a third grade fluid in a pipe. Int J Non-Linear Mech. 1995;30:687–99.
[21] Abbasbandy S, Hayat T, Ellahi R, Asghar S. Numerical results of a flow in a third grade fluid between two porous walls. Z Naturforschung A. 2009;64:59–64.
[22] Yürüsoy M. Similarity solutions to boundary layer equations for third-grade non-Newtonian fluid in special coordinate system. J Theor Appl Mech. 2003;41:775–87.
[23] Ogunsola AW, Peter BA. Effect of variable viscosity on third grade fluid flow over a radiative surface with Arrhenius reaction. Int J Pure Appl Sci Technol. 2014;22:1.
[24] Akinshilo AT, Sobamowo GM. Perturbation solutions for the study of MHD blood as a third grade nanofluid transporting gold nanoparticles through a porous channel. J Appl Comput Mech. 2017;3:103–13.
[25] Aksoy Y, Pakdemirli M. Approximate analytical solutions for flow of a third-grade fluid through a parallel-plate channel filled with a porous medium. Transp Porous Media. 2010;83:375–95.
[26] Pakdemirli M, Yilbas B. Entropy generation for pipe flow of a third grade fluid with Vogel model viscosity. Int J Non-Linear Mech. 2006;41:432–37.
[27] Pakdemirli M, Yilbas B. Entropy generation in a pipe due to non-Newtonian fluid flow: Constant viscosity case. Sadhana. 2006;31:21–9.
[28] Jayeoba O, Okoya S. Approximate analytical solutions for pipe flow of a third grade fluid with variable models of viscosities and heat generation/absorption. J Nigerian Math Soc. 2012;31:207–27.
[29] Ali N, Nazeer F, Nazeer M. Flow and heat transfer analysis of an Eyring–Powell fluid in a pipe. Z für Naturforschung A. 2018;73:265–74.
[30] Makinde OD. Laminar falling liquid film with variable viscosity along an inclined heated plate. Appl Maths Comput. 2006;175:80–8.
[31] Tshehla M. The flow of a variable viscosity fluid down an inclined plane with a free surface. Math Probl Eng. 2013;2013:8–12.
[32] Liao S. Beyond perturbation: introduction to the homotopy analysis method. London: Chapman and Hall/CRC; 2003.
[33] Kumar Sharma B, Gandhi R. Entropy-driven optimization of radiative Jeffrey tetrahybrid nanofluid flow through a stenosed bifurcated artery with Hall effects. Phys Fluids. 2023;35.
[34] Ali F, Hou Y, Zahid M, Rana M, Kumam P, Sitthithakerngkiet K. Numerical analysis of heat transfer and magnetohydrodynamic flow of viscoelastic Jeffery fluid during forward roll coating process. Heat Transf. 2023;52:911–35.
[35] Hou Y, Feng X, Zahid M, Rana M, Souayeh B. Theoretical and numerical investigation of the carreau fluid model during a non-isothermal roll coating process: a comparative study. Case Stud Therm Eng. 2023;51:103503.
[36] Ali F, Zahid M, Hou Y, Manafian J, Rana M, Hajar A. A theoretical study of reverse roll coating for a non-isothermal third-grade fluid under lubrication approximation theory. Math Probl Eng. 2022;2022.